

Unimolecular reactions in isolated and collisional systems: Deuterium isotope effect in the photoisomerization of stilbene

Scott H. Courtney, Michael W. Balk, Laura A. Philips, Steven P. Webb, Ding Yang, Donald H. Levy, and Graham R. Fleming

Citation: *The Journal of Chemical Physics* **89**, 6697 (1988); doi: 10.1063/1.455342

View online: <http://dx.doi.org/10.1063/1.455342>

View Table of Contents: <http://scitation.aip.org/content/aip/journal/jcp/89/11?ver=pdfcov>

Published by the [AIP Publishing](#)

Articles you may be interested in

[Femtosecond laser studies of the cisstilbene photoisomerization reactions](#)

J. Chem. Phys. **98**, 6291 (1993); 10.1063/1.464824

[Evidence for dynamical solvent dielectric effects: Photoisomerization of stilbenes](#)

AIP Conf. Proc. **172**, 634 (1988); 10.1063/1.37495

[Unimolecular reactions of isolated, collisional gas phase and solvated molecules: Connections between stilbene isomerization rates under supersonic jet and thermal gas phase conditions](#)

AIP Conf. Proc. **146**, 604 (1986); 10.1063/1.35907

[Photoisomerization of stilbene in low viscosity solvents: Comparison of isolated and solvated molecules](#)

J. Chem. Phys. **83**, 215 (1985); 10.1063/1.449811

[Collisional Energy Transfer in Thermal Unimolecular Systems. Dilution Effects and Falloff Region](#)

J. Chem. Phys. **48**, 1282 (1968); 10.1063/1.1668794



Unimolecular reactions in isolated and collisional systems: Deuterium isotope effect in the photoisomerization of stilbene

Scott H. Courtney,^{a)} Michael W. Balk,^{a)} Laura A. Philips,^{b)} Steven P. Webb,^{c)}
Ding Yang, Donald H. Levy, and Graham R. Fleming^{d)}

Department of Chemistry and The James Franck Institute, The University of Chicago, Chicago, Illinois 60637

(Received 8 July 1988; accepted 16 August 1988)

The isomerization of *t*-stilbene (stilbene h_{12}) and three deuterated derivatives has been studied in a supersonic expansion, the thermal gas phase, and solution. In the jet we find that almost all effect of full deuteration (stilbene d_{12}) is produced by deuteration of the two ethylinic hydrogens only (stilbene d_2). Complete deuteration of the phenyl rings (stilbene d_{10}) has rather little influence on the decay of the jet-cooled molecule. Nonexponential decays are found at intermediate excess energies in the jet-cooled system, with the degree of nonexponentiality decreasing with increasing excess energy. The ordering of the decay rates observed in the jet is not consistent with previous RRKM calculations of the isomerization rates of stilbene h_{12} and d_2 . Using similar parameters the calculations consistently place the stilbene d_2 and stilbene d_{10} curves in the wrong order. Our results suggest extensive but not complete vibrational relaxation in the isolated molecule. Vibrational redistribution rapidly becomes complete in the presence of buffer gas. In thermal samples the isomerization rates of stilbene h_{12} and stilbene d_{10} are identical over a wide range of solvents and temperatures. By contrast the isomerization rates in stilbene d_2 and stilbene d_{12} are 1.4 and 1.5 times slower than in stilbene h_{12} . Again, these ratios appear constant over a wide range of experimental conditions.

I. INTRODUCTION

The fact that the isomerization of *t*-stilbene can be studied over the range of environment from supersonic molecular beams through the gas phase to both polar and nonpolar solutions has made this system a test case for theories of activated barrier crossing. The supersonic jet data have been discussed by Troe^{1,2} and by Zewail and co-workers^{3,4} in the context of RRKM theory. RRKM theory is able to describe the dependence of rate on excess energy $k(E)$ for perprotero *t*-stilbene (stilbene h_{12}) very well, although there does not seem to be a consensus on whether an adiabatic or nonadiabatic approach should be used.¹⁻⁴ Felker *et al.*³ showed that if the nonadiabatic approach was used and parameters derived which fit $k(E)$ for stilbene h_{12} , then a good fit to $k(E)$ for perdeutero *t*-stilbene (stilbene d_{12}) could be obtained simply by changing the appropriate frequencies and leaving the nonadiabaticity parameter unaltered. In this picture the lower rate observed for stilbene d_{12} arises simply from the higher density of states at a given excess energy, and RRKM theory appears to account successfully for the observed behavior.

On going from the approximate microcanonical ensemble of the supersonic jet to a thermalized but still isolated molecule, Balk and Fleming⁵ found that the nonexponential fluorescence decay observed for excitation near the origin could be described very well by a simple thermal average of $k(E)$. This procedure leads to an experimental estimate

$k(T)$ of $k_{\text{TST}}(T)$, the transition state rate constant. However, contrary to expectation, for buffer gas pressures above 2 atm the isomerization rate was found to exceed $k(T)$, rising to about 10 times $k(T)$ at 100 atm. This suggests that the jet rates may differ from the microcanonical rates and/or that some other "nonstatistical" effect is operative in the collision dynamics.⁶⁻⁸ The interpretation of the collisional data is made more complex by the possibility of collisional isoenergetic redistribution of vibrational energy in addition to inelastic vibrational relaxation. For states with energy around the barrier height (1250 cm⁻¹) Felker *et al.*³ suggest an IVR time scale of 20–50 ps as compared with hard sphere collision times for stilbene methane collisions of 40–8 ps in the 1 to 5 atm pressure range. Thus, the possibility of incomplete vibrational redistribution should be considered in interpreting both the jet data and the low pressure gas phase data.

In order to investigate the influence of vibrational level structure and densities of states on the isomerization dynamics, we have studied two further isotopically modified stilbenes— α,α' dideuterostilbene (stilbene d_2) and 2,2',3,3',4,4',5,5',6,6' deca deuterostilbene (stilbene d_{10}), in addition to stilbene h_{12} and stilbene d_{12} . Experiments were carried out in supersonic expansions, low pressure gases, and in solution over a wide temperature range. The data show that essentially the full effect of complete deuteration is achieved in stilbene d_2 . Deuteration of the phenyl rings (stilbene d_{10}) has a small effect on $k(E)$ and no detectable influence on $k(T)$ over a wide range of solvents and temperatures. The jet data cast serious doubt on earlier conclusions about the applicability of RRKM theory to the isomerization process. We have not been successful in finding a consis-

^{a)} Present address: AT&T Bell Laboratories, Murray Hill, N.J. 07974.

^{b)} Present address: Department of Chemistry, Cornell University, Ithaca, N.Y. 14853

^{c)} Present address: Dow Chemical Midland, MI 48640

^{d)} John Simon Guggenheim Fellow.

tent set of parameters for RRKM calculations that reproduce $k(E)$ for all four molecules.

II. EXPERIMENTAL

A. Materials

Deuterated *trans*-stilbenes were synthesized by means of sodium and liquid ammonia reduction of alkynes, which generally gave the *trans*-alkene with high specificity.^{9–11}

Trans-stilbene- d_2 , prepared accordingly from Na-liquid ND_3 (MSD isotopes) and diphenyl acetylene in 3:1 mole ratio at -70° to -35° , with due care in decomposing the excess sodium at the end of 60 min by deuterated ethanol and dilute ND_4OD , was recrystallized twice from benzene-hexane for the present studies. (Overall yield, 83%; m.p. 125.5–126 °C, IR max at 1602 cm^{-1} , 909 cm^{-1} , NMR in CDCl_3 : phenyl protons only, triplet at 7.22 ppm, triplet at 7.33 ppm, and doublet at 7.49 in ratio of 1:2:2; mass spect: m/e at 182; percentage of deuteration, estimated to be $>98\%$ on the basis of NMR and mass spectral analyses.)

Trans-stilbene d_{10} , prepared from Na-liquid NH_3 and tolan d_{10} ,^{9–11} with excess sodium decomposed by NH_4NO_3 and dilute NH_4OH in the usual manner, was purified by column chromatography (silica gel, activity 1 benzene-hexane 1:4 mixture) to remove traces of the diphenylethane contaminant, after which it was recrystallized twice from benzene-hexane to give a pure product. (Overall yield, 53%; m.p. 125–126 °C; IR max at 962 cm^{-1} , “diagnostic” for *trans*-alkene¹¹; NMR in CDCl_3 : vinyl proton only, singlet at 7.13 ppm; mass spect: m/e at 190; percentage of deuteration, estimated to be $>98\%$ on the basis of NMR and mass spectral analyses.)

Trans-stilbene h_{12} (Kodak scintillation grade) which was shown to be over 99% pure by NMR, mass spectral analyses and HPLC, was used without purification. No dependence of the fluorescence spectrum on excitation wavelength was observed.

Ethane (Matheson research grade) and propane (Phillip research grade) were used as stated.

B. Time correlated single photon counting

Fluorescence lifetimes were determined by single photon counting. We have recently described this technique in detail¹² and here we only discuss recent improvements and details specific to these measurements.

The excitation source was a cavity dumped dye laser (Coherent 599) synchronously pumped by a mode-locked argon ion laser. The dye laser pulses (approximately 10 ps in duration) were frequency doubled using birefringent crystals. The dye laser pulses are monitored using a real time spinning autocorrelator. We use an Ortec 457 time to amplitude converter (TAC) whose output is sent to a multichannel analyzer (Tracor-Northern TN-7200) running in pulse height analysis mode. The data was transferred to either a Celerity minicomputer or a microVAX for storage and iterative reconvolution.

In the supersonic jet expansion and thermal vapor experiments, the “stop” signal to the TAC was provided by a portion of the laser pulse train (picked off by a beam split-

ter) and sent to a fast photodiode (Telefunken BPW28). The anode pulse from a microchannel plate (MCP) was the “start” signal. The solution phase measurements were performed using the “forward” counting configuration.

We utilized a new design MCP with 6 μm channels (Hamamatsu R2809U) for the jet measurements. In comparison to our older MCP (Hamamatsu R1645U-01 and ITT F4129 which gave instrument response functions approximately 70–100 ps FWHM), we can achieve slightly narrower instrument functions using the new tube. For example, Fig. 1 shows a good fit with a 60 ps FWHM instrument functions using an HP 8447E amplifier and a Tennelec TC455 discriminator. We have tried using very high bandwidth amplifiers (dc to 8 GHz) and found no significant improvement.

C. Supersonic jet expansion

A detailed description of the supersonic jet apparatus¹³ with single photon counting detection¹⁴ is found elsewhere, and thus will only be briefly described here. The dye laser was cavity dumped at 3.8 MHz and frequency doubling was accomplished with a 2 mm KDP crystal. In these experiments the sample, supported on cotton and located immediately behind the 25 μm nozzle, was heated via a standard oven to 90 °C. Helium was used as a carrier gas at 18 atm. Great care was taken to minimize the consumption of the deuterated samples. Therefore, conditions were established so that for each experiment only 20–30 mg of material were required. The laser crossed the jet at approximately 200 noz-

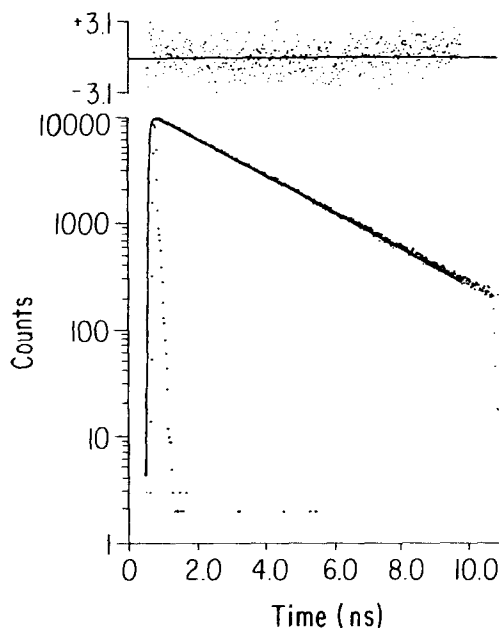


FIG. 1. Time-resolved, single exponential decay for stilbene h_{12} measured as the total fluorescence from excitation at 32 248 cm^{-1} ($E_x = 21 \text{ eV}$). As with all excitations well below the barrier to isomerization, the fluorescence decay yields the radiative lifetime in the absence of isomerization of $2.5 \pm 0.1 \text{ ns}$ [$\Phi_f = 1.0$ (Ref. 15)]. The instrument response (dotted peak below the data) was obtained by laser scattering from argon clusters in a separate experiment. The fit (solid line through the data) is composed of a single exponential decay of 2.53 ns convoluted with the instrument response. The differences between the data and the fit are shown at the top of the figure in the form of normalized residuals.

zle diameters downstream of the 25 μm nozzle. Instrument functions were measured by scattering the excitation laser from argon clusters generated by expanding argon through a 25 μm nozzle with 90 atm of backing pressure. The total fluorescence was collected in these experiments. Excitation wavelength was monitored for each measurement by sending the fundamental laser light into a monochromator. Excitation frequencies were selected based on literature values for vibronic transitions when available, otherwise the excitation laser was scanned for a maximum at the detector.

D. Thermal vapor

LiIO_3 was used to produce the second harmonic of a Kiton Red modelocked dye laser cavity dumped at 3.8 MHz. The laser fundamental wavelength was 620 nm with a bandwidth of ≈ 0.5 nm FWHM. The sample cell and vacuum system (10^{-5} Torr) were always rinsed with buffer gas (Methane, Matheson) before the cell was brought to the desired pressure. We utilized a standard quartz cuvette to a maximum pressure of 5 atm.

E. Solution phase

The excitation source was the second harmonic of a R6G synchronously mode locked dye laser. In this case we used forward counting by cavity dumping at 76 kHz. The excitation wavelengths used were 300 and 313 nm. The fluorescence was detected through a polarizer at the "magic angle" and acceptable fits were obtained to single exponential decays. In most cases the sample was in normal 1 cm fused silica cuvettes set in a cell block with a Neslab RTE-8 circulating water/ethylene glycol to regulate the temperature. For the low temperature measurements, a Neslab ULT-80 bath circulated a water/methanol mixture through the cell mount. In both cases the temperature was monitored with a calibrated thermocouple/digital thermometer combination. The estimated accuracy of the sample temperature was $\pm 1^\circ\text{C}$ and the temperature range studied was 42 to -57°C . The cell block and detection optics were under nitrogen to prevent condensation. The instrument functions were obtained using light scattered from a suspension of a nondairy creamer.

II. Results

A. Supersonic jet expansion

The excess energy dependence of the fluorescence lifetime was studied over a range of about $30\,000\text{ cm}^{-1}$ for stilbene h_{12} , d_2 , and d_{10} . Zewail and co-workers^{3,4} have previously studied stilbene h_{12} and d_{12} over this range and our results were in good agreement with these workers for the h_{12} data. In order to accurately compare the excess energy dependence the energy of the origin transition was determined for the three molecules. The values are listed in Table I along with the h_{12} and d_{12} values from Ref. 4. Also listed in Table I is the fluorescence lifetime of the vibrationless excited state which is taken to be the inverse of the radiative rate since the fluorescence yield is reported to be unity.¹⁵ For low excess energies the fluorescence decays were all single exponential, Fig. 1 gives a typical example for stilbene h_{12} . As the

TABLE I. Origin transitions and radiative lifetimes for the four stilbenes.

Compound	$E_{0,0}$ (cm^{-1})	τ_F (ns) ^a
h_{12}	32 227 (32 244) ^b	2.52 (2.67)
d_2	32 248	2.56
d_{10}	32 311	2.48
d_{12}	32 224 (32 336)	... (2.53)

^a Average lifetime measured at less than 500 cm^{-1} above the origin. Note that the fluorescence was detected "broadband".

^b The values in parentheses are from Ref. 4.

excess energy is increased the fluorescence decay remains single exponential with a constant lifetime until $E_x = 800\text{--}1000\text{ cm}^{-1}$. Now the decay time shortens and the decays become nonexponential (Fig. 2). The decay curves fit well to a sum of two exponential components and the results of such fits are given in Tables II, III, and IV for stilbene h_{12} , d_2 , and d_{10} , respectively. As E_x is further increased the amplitude of the second component becomes very small ($\leq 1\%$). A typical curve for $E_x = 2729\text{ cm}^{-1}$ in d_2 is shown in Fig. 3.

In order to define a consistent rate, since in the intermediate E_x range in particular the amplitudes and decay times of the two components are strongly correlated, we set

$$k_{\text{nr}}^* = (a_1\tau_1 + a_2\tau_2)^{-1} - k_{\text{rad}}. \quad (1)$$

Values of k_{nr}^* are listed in Tables II–IV and shown in Fig. 4, along with data from Zewail and co-workers for h_{12} and

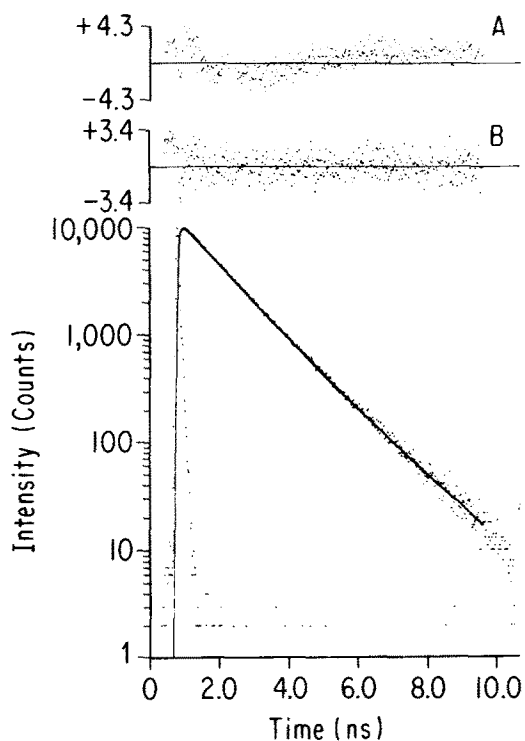


FIG. 2. Time-resolved, nonexponential decay of stilbene d_{10} , measured as the total fluorescence from excitation at $33\,727\text{ cm}^{-1}$ ($E_x = 1416\text{ cm}^{-1}$). The solid curve is a fit to a sum of two exponentials ($a_1 = 0.47$, $\tau_1 = 1.00$ ns, $a_2 = 0.53$, $\tau_2 = 1.49$ ns). The residuals are shown for a single exponential fit (upper curve, $\chi_R^2 = 2.2$) and the double exponential fit (lower curve, $\chi_R^2 = 1.2$).

TABLE II. Nonradiative decay rates as a function of energy for stilbene h_{12} .

$E - E_{0-0}$ (cm ⁻¹)	A_1	τ_1 (ns)	A_2	τ_2 (ns)	k_{nr}^* (ns ⁻¹) ^a
21	100.0	2.53	0.0
52	100.0	2.52	0.0
94	100.0	2.54	0.0
125	100.0	2.51	0.0
225	100.0	2.52	0.0
293	100.0	2.51	0.0
421	100.0	2.50	0.0
496	100.0	2.47	0.01
689	100.0	2.43	0.02
743	100.0	2.44	0.01
765	100.0	2.40	0.02
864	64.0	2.66	36.0	1.67	0.04
985	71.0	2.46	29.0	1.33	0.07
1062	68.7	2.41	31.3	1.34	0.08
1184	62.1	2.15	37.9	1.13	0.17
1263	54.5	1.94	45.5	1.10	0.24
1330	48.0	1.75	52.0	1.00	0.34
1466	64.0	0.823	36.0	1.40	0.56
1466	76.6	0.876	23.0	1.62	0.57
1660	82.8	0.616	17.0	1.13	1.02
1856	95.0	0.452	5.0	1.18	1.65
1856	87.6	0.445	12.4	0.882	1.61
2031	93.7	0.347	6.3	0.812	2.26
2196	96.7	0.267	3.3	0.852	3.00
2447	98.4	0.202	1.6	0.867	4.30
2665	98.9	0.159	1.1	0.758	5.63
2861	99.1	0.132	0.9	0.617	6.96

^aThe value tabulated has the average fluorescence rate near the 0-0 subtracted (see Table I) and is a simple weighted average for the double exponential fits.

TABLE III. Nonradiative decay rates as a function of energy for stilbene d_2 .

$E - E_{0-0}$ (cm ⁻¹)	A_1	τ_1 (ns)	A_2	τ_2 (ns)	k_{nr}^* (ns ⁻¹) ^a
-11	100.0	2.53	0.01
31	100.0	2.56	0.0
73	100.0	2.54	0.0
83	100.0	2.56	0.0
178	100.0	2.59	0.0
220	100.0	2.55	0.0
220	100.0	2.56	0.0
283	100.0	2.56	0.0
378	100.0	2.60	-0.01
539	100.0	2.53	0.01
668	100.0	2.54	0.0
975	100.0	2.50	0.01
1152	100.0	2.34	0.04
1163	100.0	2.35	0.04
1208	100.0	2.11	0.08
1309	57.8	2.17	48.2	1.42	0.16
1343	60.9	2.39	39.1	1.54	0.10
1411	52.5	1.95	47.5	1.23	0.23
1502	56.8	1.25	43.2	1.69	0.30
1650	64.9	0.846	35.1	1.36	0.58
1650	59.5	0.815	40.5	1.35	0.58
1696	97.0	1.00	3.0	2.55	0.56
1777	65.0	0.733	35.0	1.10	0.77
1882	86.0	0.644	14.0	1.08	1.03
1999	91.0	0.515	9.0	1.05	1.39
1999	97.0	0.551	3.0	1.86	1.30
2128	99.0	0.483	0.6	3.97	1.60
2235	94.0	0.383	6.0	0.794	2.06
2354	97.0	0.333	3.0	0.749	2.51
2438	98.0	0.301	2.0	0.744	2.84
2571	98.0	0.256	2.0	0.634	3.40
2729	99.7	0.217	0.3	1.24	4.15

^aThe value tabulated has the average fluorescence rate near the 0-0 subtracted (see Table I) and is a simple weighted average for the double exponential fits.

TABLE IV. Nonradiative decay rates as a function of energy for stilbene d_{10} .

$E - E_{0-0}$ (cm^{-1})	A_1	τ_1 (ns)	A_2	τ_2 (ns)	k_{nr}^* (ns^{-1}) ^a
-32	100.0	2.48	0.0
-11	100.0	2.51	0.0
41	100.0	2.47	0.0
209	100.0	2.48	0.0
444	100.0	2.46	0.0
551	100.0	2.46	0.0
649	100.0	2.36	0.02
758	100.0	2.39	0.02
857	80.9	2.17	19.1	3.14	0.02
945	68.0	2.53	32.0	1.64	0.04
1045	68.0	1.89	32.0	2.82	0.05
1156	60.0	2.10	40.0	1.18	0.17
1235	66.0	1.97	34.0	1.15	0.19
1280	59.0	1.71	41.0	2.58	0.08
1416	53.0	1.49	47.0	1.00	0.39
1416	98.0	1.23	2.0	6.17	0.35
1541	94.0	0.929	6.0	2.05	0.60
1622	77.5	0.717	22.5	1.19	0.81
1714	93.0	0.681	7.0	1.33	0.97
1761	87.0	0.569	13.0	1.06	1.18
1761	91.0	0.593	9.0	1.29	1.12
1900	98.0	0.516	2.0	1.91	1.44
2041	95.0	0.394	5.0	0.977	1.96
2172	97.0	0.347	3.0	1.11	2.30
2569	99.0	0.218	1.0	1.17	4.00
2715	99.0	0.184	1.0	0.979	4.81
2838	99.0	0.162	1.0	0.788	5.55
2962	99.0	0.144	1.0	0.772	6.27
3062	99.0	0.134	1.0	0.818	6.69

^aThe value tabulated has the average fluorescence rate near the 0-0 subtracted (see Table 1) and is a simple weighted average for the double exponential fits.

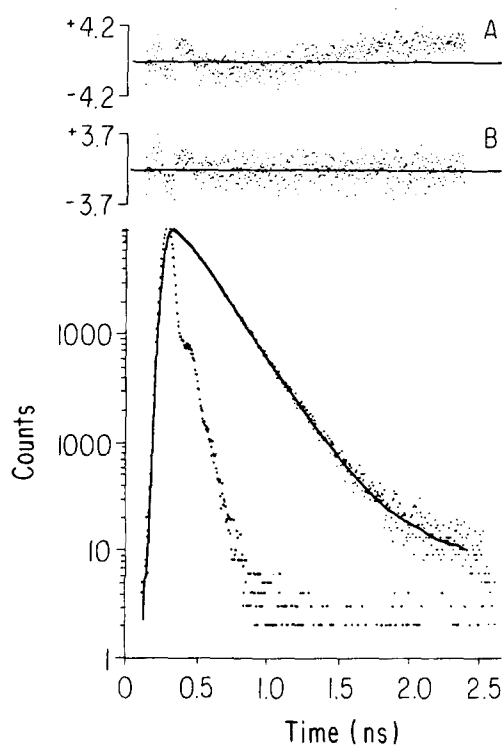


FIG. 3. Time-resolved, nonexponential decay of stilbene d_2 measured as the total fluorescence from excitation at $34\,977\text{ cm}^{-1}$ ($E_x = 2729\text{ cm}^{-1}$). The short decay time (> 99%, 220 ps) reflects the contribution from the nonradiative isomerization process. The instrument response (dotted curve below the data) and the fit (solid line) are also shown in the figure. The differences between the data and the fit in the form of normalized residuals are shown at the top of the figure (curve B) and can be compared to the nonrandom residuals from a single exponential fit (curve A).

d_{12} ⁴ (although these authors reported only single exponential decay times our k_{nr}^* values are in quite good agreement with their k_{nr}^* values for stilbene h_{12}). The large variations possible in A_1 and τ_1 and A_2 and τ_2 are shown, for example, by the two entries for E_x 1416 cm^{-1} for stilbene d_{10} in Table IV. k_{nr}^* is, however, the same for both sets of parameters.

The order of the experimental curves in Fig. 4 does not conform to expectations based on density of states arguments. This order (at a given E_x) is $k(h_{12}) > k(d_{10}) > k(d_2) > k(d_{12})$. Shown in the upper panel of Fig. 4 are the results of nonadiabatic RRKM calculations (using the frequencies listed in Table V), assuming a constant nonadiabaticity parameter ($\gamma' = 0.27$ ³) and unchanged frequencies in the transition state. The experimental h_{12} and d_{12} curves are reproduced quite well, but the d_2 and d_{10} curves are in the *wrong order* with the calculated d_{10} and d_{12} curves lying close together and d_2 lying close to h_{12} .

B. Thermal vapor

The fluorescence decay of the stilbene isomers, under thermal conditions but at very low pressures where there are no collisions during the excited state lifetimes is highly nonexponential. The curves labeled HV and DV in Fig. 5 show data for h_{12} and d_{12} excited near the origin in order to produce an initial rovibrational distribution in the excited state which closely approximates the original ground state Boltzmann distribution.⁵

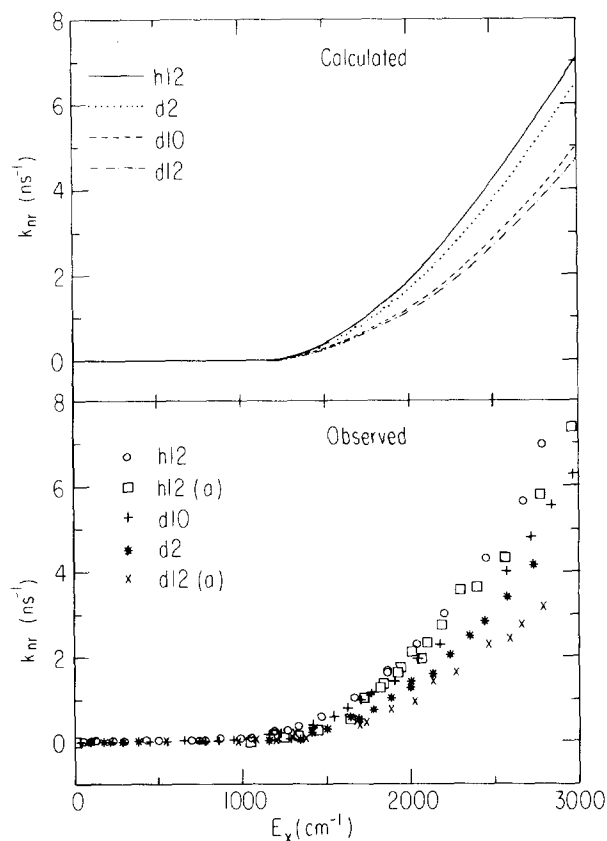


FIG. 4. Top—Nonadiabatic RRKM calculations using the expression of Felker and Zewail³ and the frequencies described in the text. Bottom—Observed nonradiative decay rates for the four stilbene isomers. (a) The values obtained in Ref. 3 for h_{12} and d_{12} are included for comparison. Notice that the ordering of the d_2 and d_{10} isomers are reversed relative to the calculation.

The qualitative picture behind the nonexponential decay is apparent. The hot molecules decay rapidly leading to a progressive cooling of the ensemble. At long times only molecules with insufficient energy to isomerize are left and the decay approaches the radiative lifetime. Quantitatively Balk and Fleming⁵ were able to describe the collision-free fluorescence decay in h_{12} by simply summing the (exponential) decays for each level (obtained from the jet data), weighted by their initial relative populations. As the buffer gas (methane) pressure is increased, the fluorescence decay becomes more nearly exponential. For pressures above 2 atm the decays are single exponential over two decades and as the buffer gas pressure is increased the observed lifetimes decrease monotonically. Figure 5 shows data for h_{12} and d_{12} at 1 atm and 5 atm methane buffer gas in addition to the very low pressure results. In contrast to the jet data the isolated molecule curves are very similar for the two isotopes (although d_{12} consistently decays slightly faster than h_{12}). However, as the buffer pressure is increased the order of the decays reverts to the jet result. Figure 6 summarizes our data for all four molecules over the methane pressure range 1–5 atm. The inverse of the lifetime is linearly related to pressure over this range. The h_{12} and d_{10} data are identical within our experimental error, whereas the d_2 data consistently lie at slightly higher rates than the d_{12} data.

TABLE V. Reactant frequencies used in RRKM calculation.

h_{12}	d_2	d_{10}	d_{12}
3092	3088	2305	2303
3090	3088	2308	2307
3080	3078	2297	2297
3088	3085	2306	2305
3086	3081	2299	2299
3078	2270	3077	2269
1671	1638	1667	1627
1606	1602	1567	1567
1566	1562	1529	1529
1523	1521	1407	1397
1500	1500	1376	1374
1460	1457	1407	1407
1392	1069	1383	1068
1321	1322	1043	1043
1264	1260	1216	1216
1177	1172	860	862
1155	1154	840	839
1086	1105	837	848
1041	1050	809	809
1036	1034	994	993
915	847	748	749
700	688	680	675
654	653	629	629
309	306	292	292
230	219	211	211
1012	1002	874	859
1003	1001	812	809
903	659	884	667
800	799	684	665
834	832	655	655
715	688	534	532
603	600	535	533
445	444	444	443
401	397	397	397
289	260	264	250
131	130	121	121
1006	1005	806	806
999	995	793	797
906	672	906	671
888	893	742	731
797	797	623	623
721	721	518	517
611	608	571	570
469	465	409	407
396	396	374	373
238	238	237	237
55	55	54	54
41	41	41	41
3095	3095	2288	2287
3091	3092	2288	2289
3090	3089	2294	2293
3088	3087	2294	2294
3087	3086	2298	2289
3084	2288	3089	2285
1662	1662	1626	1630
1581	1578	1544	1540
1543	1541	1426	1430
1535	1529	1437	1402
1484	1462	1433	1425
1396	1374	1082	1087
1377	1146	1382	1168
1306	1270	1324	1279
1174	1173	858	854
1157	1156	847	844
1090	1083	845	839
1046	1030	829	827
1021	1002	963	961
862	848	796	796
668	611	548	549
593	552	525	519
548	450	500	500
88	87	87	87

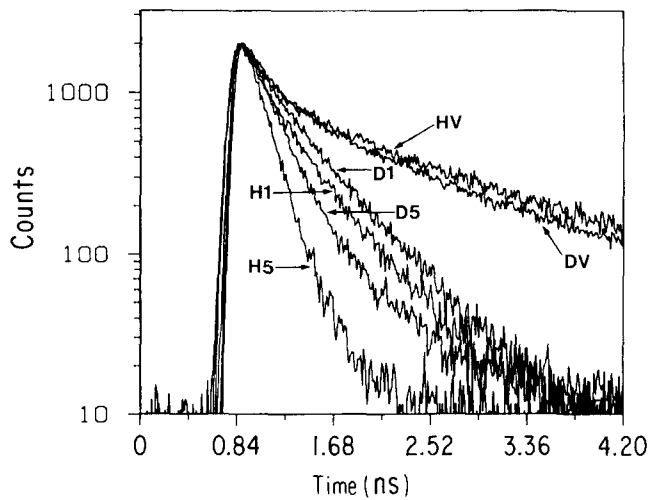


FIG. 5. Comparison of stilbene h_{12} and stilbene d_{12} transient fluorescence decay curves (< 1 mTorr) and stilbene plus methane in the gas phase. All measurements are at 296 K. HV = stilbene h_{12} vapor; DV = stilbene d_{12} vapor; H1 = stilbene h_{12} in 1 atm methane; D1 = stilbene d_{12} in 1 atm methane; H5 = stilbene h_{12} in 5 atm methane; D5 = stilbene d_{12} in 5 atm methane.

C. Solution phase

At 5 atm methane buffer gas the decay rates of h_{12} and d_{10} are about 1.3 times faster than those of d_{12} and d_2 . Since the Kramers turnover does not occur until about 100 atm pressure^{6,7,8,16} the difference between the decay rates would be very large if the curves continued to diverge at the same rate. In fact by 5 atm, the curves have almost reached their limiting separation. Figure 7 shows a comparison of h_{12} and d_{12} (A) and d_{10} and d_2 (B) in hexane solution. All the decays are single exponential. At 23 °C the ratio of decay times for h_{12} and d_{12} is 1.49 and at 6 °C the ratio for d_{10} and d_2 is 1.47.

A number of studies have shown that isomerization of stilbene is much faster in an alcohol solution of given viscos-

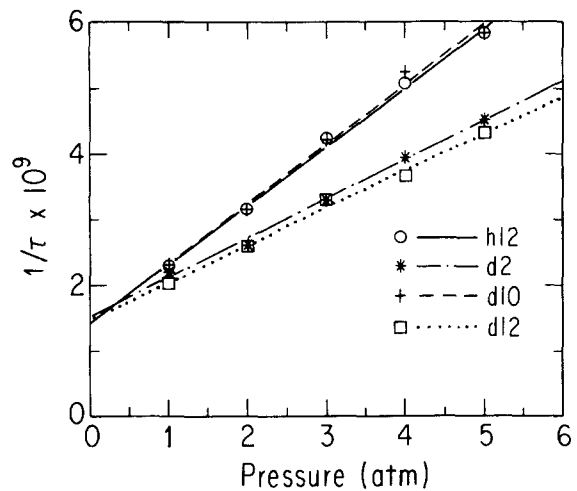


FIG. 6. Nonradiative rates observed for the four stilbene isomers with methane buffer gas present. The rates are weighted averages from double exponential fits (see the text for the details). \circ h_{12} , $*$ d_2 , $+$ d_{10} , \square d_{12} .

ity than in an alkane solution of the same viscosity.¹⁷⁻¹⁹ However, the ratios of rates between the isomers are almost completely insensitive to a change to polar solution. For example, in methanol at 24 °C the lifetimes of h_{12} and d_{12} are 42.6 and 66.1 ps, respectively, giving a ratio of 1.48. Table VI summarizes data in hexane, methanol, and propanol. In all cases, $\tau(h_{12}) = \tau(d_{10})$ within our precision (± 2 ps), but $\tau(d_2)$ is consistently slightly shorter than (d_{12}).

The differences in decay rate observed for the different isomers might simply be due to a difference in barrier height. If this were the case temperature dependent studies should reveal differing activation energies, providing the temperature range is large enough. Figure 8 shows Arrhenius plots for all four isomers in propanol solution over a temperature range of ~ 100 °C. The slopes for h_{12} , d_{10} , and d_{12} are identical within our experimental error, the slope for d_2 is slightly larger than for the other three compounds in this particular solvent. Arrhenius parameters for hexane, propanol, and

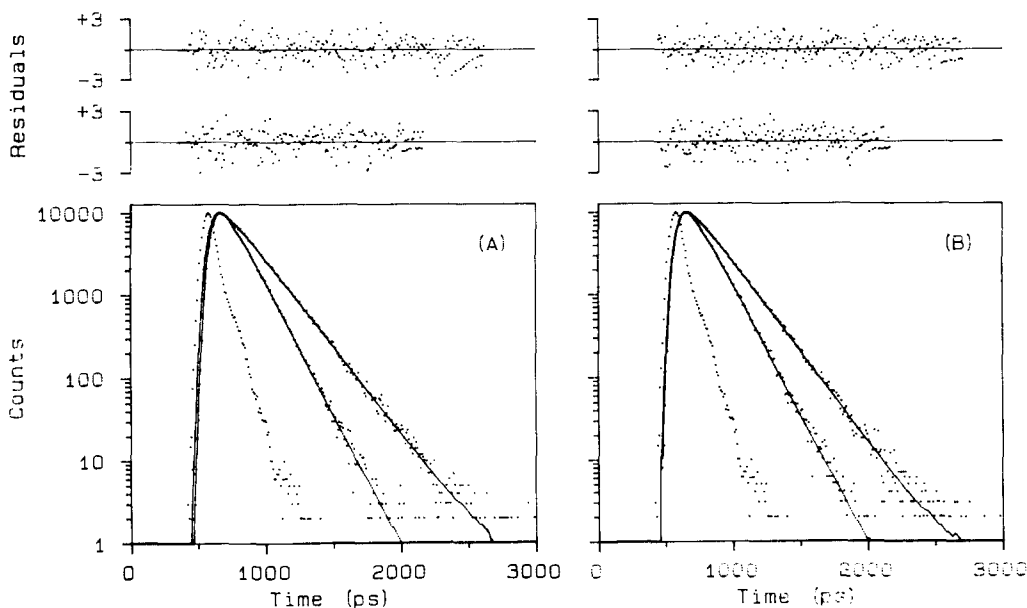


FIG. 7. (a) Fluorescence decays of stilbene d_{12} (upper curve) and stilbene h_{12} (lower curve) in n -hexane at +6 °C. Single exponential fits give $\tau = 204$ ps and $\tau = 131$ ps, respectively. (b) Fluorescence decays of stilbene d_2 (upper curve) and stilbene d_{10} (lower) in n -hexane at +6 °C. The single exponential fits yield $\tau = 197$ ps and $\tau = 134$ ps, respectively. The instrument response function was approximately 100 ps FWHM.

TABLE VI. Comparison of selected *trans*-stilbene isotopes solution phase lifetimes.

T (K)	η (cp)	h_{12} τ_f (ps)	d_2 τ_f (ps)	d_{10} τ_f (ps)	d_{12} τ_f (ps)
Hexane					
296	0.307	82.9	119.2	82.7	123.3
240	0.607	308.9	450.1	308.7	462.5
229	0.721	411.1	564.7	422.8	637.9
216	0.905	570.1	753.5	569.4	771.7
Methanol					
297	0.56	42.6	61.1	44.1	63.1
247	1.32	149.6	210.3	154.5	222.4
230	1.92	253.3	346.7	256.6	363.4
216	2.74	393.3	530.0	395.9	550.0
Propanol					
294	2.18	58.0	76.3	57.1	81.7
250	7.80	205.1	279.4	230.2	297.5
232	15.1	400.4	495.8	379.4	522.0
220	25.0	526.8	664.3	531.9	693.2

methanol are given in Table VII. Within our experimental error there is no evidence for a change in activation energy between the isomers.

III. DISCUSSION

A. Supersonic jet expansion

In the isolated *t*-stilbene molecule at least two fundamental questions relating to the isomerization process have not yet been clearly answered. (1) Is energy randomization complete on the relevant time scale, so that a statistical theory such as RRKM is applicable to the dynamics? (2) If RRKM is appropriate, should the process be considered as adiabatic or nonadiabatic? This latter issue has been recently discussed.^{2,3} Equally good fits to the stilbene h_{12} $k(E)$ data in supersonic expansions have¹⁻⁴ been obtained by adiabatic or nonadiabatic approaches. A recent calculation²⁰ supports an adiabatic reaction surface. A simple RRKM calculation

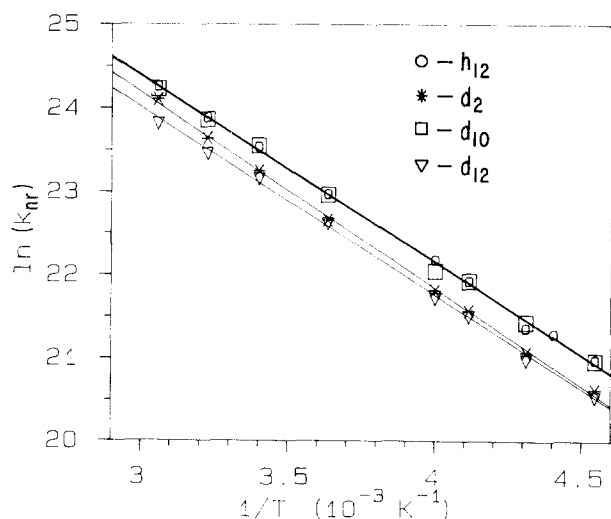


FIG. 8. Arrhenius plots for the four stilbene isomers in propanol. See Table V for the parameters. \circ h_{12} , $*$ d_2 , \square d_{10} , ∇ d_{12} . In all the liquid conditions studied, the rates determined for h_{12} and d_{10} were indistinguishable.

selecting a reaction coordinate frequency and leaving all other frequencies unchanged produces rates that are substantially faster than the experimental value. Zewail and Felker³ introduced an adiabaticity parameter γ in order to lower the calculated rates. Troe,^{1,2} on the other hand, assumed the isomerization was adiabatic and reduced the calculated rates by increasing the frequency of one or more modes in the transition state. (It should also be noted that the two calculations used significantly different values of the reaction coordinate frequency, 88 vs 400 cm^{-1} .^{3,4} The lower value of the reaction coordinate frequency also leads to lower absolute rates.) Zewail and co-workers extended their nonadiabatic calculation to stilbene d_{12} and found that the $k(E)$ data could be well fit using the same adiabaticity parameter as for h_{12} , assuming unchanged transition state frequencies and changing the appropriate vibration frequencies from their values in the perprotero molecule. Thus RRKM appeared to give a successful description of the isomerization of *t*-stilbenes.

We have used the approaches of both Zewail and co-workers^{3,4} and of Troe¹ in carrying out RRKM calculations on stilbenes d_2 and d_{10} . Vibrational frequencies were obtained by using the ground state of Meic and Gusten²¹ to scale the excited state frequencies calculated by Warshel²² for stilbene h_{12} . The values of the frequencies used for all four molecules are listed in Table V.

We have already noted (see Fig. IV) that the nonadiabatic calculation (with unchanged transition state frequencies) does not reproduce the order of the four curves. A similar, incorrect, ordering is found using the adiabatic approach of Troe (his model E¹) as shown in Fig. 9. Here the $C_e - \varphi$ torsion frequency is increased by a factor of 2.15 in the transition state. Again the d_2 curve lies close to the h_{12} curve and the d_{10} close to the d_{12} curve. At this point we note that after the experiments the identity of the samples was rechecked and confirmed by NMR.

Evidently the major effect of deuteration arises from the ethylinic deuteriums and the influence of the increased density of states resulting from phenyl ring deuteration is much smaller than would be expected on the basis of a purely sta-

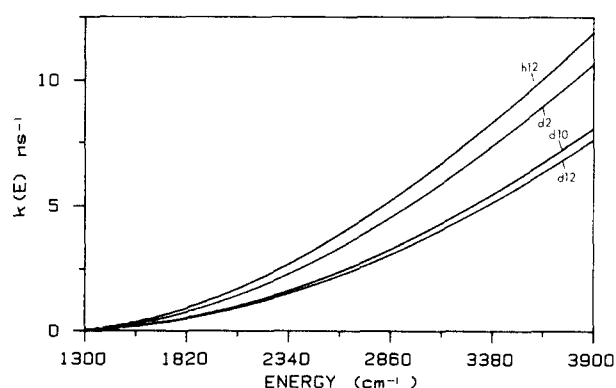


FIG. 9. RRKM calculations for the stilbene isotopes using the parameterization of Troe.¹ The reaction coordinate frequency is 88 cm^{-1} in all four molecules and the $C_e - \varphi$ torsion frequency (41 cm^{-1}) is increased by a factor of 2.15 in the transition state. All other frequencies are listed in Table V.

tistical theory. The lack of complete energy randomization is also indicated by the small amount of long lived fluorescence observed even at fairly high excess energies (Tables II–IV). Since the fluorescence near the origin is rigorously single exponential, the short component at higher energies is unlikely to be an impurity and most likely represents an intrinsically nonexponential decay process. The finding that both the amplitude and the lifetime of the long component decrease with increasing excess energy is in line with the expectation that randomization should become complete for large values of excess energy. Although a model involving extensive but not complete IVR seems consistent with our data, a number of other possibilities should be considered. First, it may be possible to “rescue” RRKM by assuming that the change in $C_e-\varphi$ torsion frequency in the transition state is substantially different for C_e-H than for C_e-D . It is not obvious, however, why deuteration on C_e or on the 2-position of the phenyl ring (i.e., d_2 vs d_{10}) would produce such different results. Recent spectroscopic studies of Spangler *et al.*²³ on stilbene d_1 indicate that in S_1 (i.e., the reactant state) the $C_e-\varphi$ torsion frequency differs very little from that in stilbene h_{12} . Second, the adiabaticity parameter could vary between the different molecules. In this case it seems that deuteration should enhance the isomerization rate, since if the relevant motion involves hydrogen (or deuterium), substitution of the heavier isotope will make the process more adiabatic (slower motion). Numerical estimates suggest that this effect should be very slight ($< 1\%$). A further possibility is that there are changes in the barrier height resulting from zero point energy differences between reactant and transition states. If this involves high frequency modes it can be modeled by simply changing the value of E_0 in the RRKM calculation. Figure 10 shows a set of calculations based on the hypothesis that ring deuteration lowers E_0 by 50 cm^{-1} and ethylenic deuteration raises E_0 by 75 cm^{-1} . In d_{12} the two effects are assumed additive. Now the ordering is correct. It would be very difficult to tell from the data in Fig. 4 or Tables II–IV if such small changes in E_0 are present, however the h_{12} and d_{10} curves (Tables II and IV) do seem distinct below $E_x \sim 1700\text{ cm}^{-1}$ which is not the case in Fig. 10. More revealing perhaps, is the finding that the

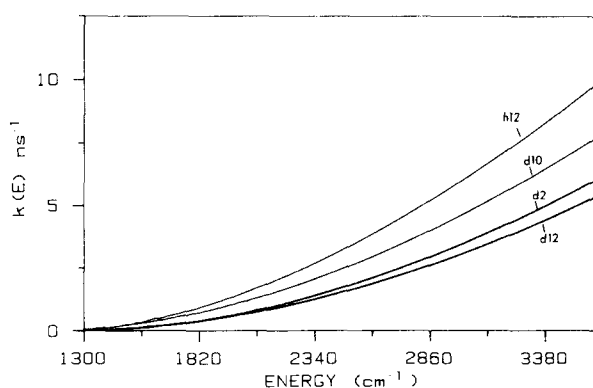


FIG. 10. RRKM calculations for the stilbene isotopes using different E_0 values for the four molecules. $E_0 = 1300\text{ cm}^{-1}$ (h_{12}), 1250 cm^{-1} (d_{10}), 1375 cm^{-1} (d_2), and 1325 cm^{-1} (d_{12}). Other parameters are as in Figure 9.

thermal average decay curves calculated for the parameters of Fig. 10 are significantly different from each other which is not the case experimentally. In addition, the Arrhenius parameters for h_{12} and d_{10} differ by only $\sim 15\text{ cm}^{-1}$ in the three solvents studied (Table VII). The d_2 and d_{12} Arrhenius parameters are not systematically higher than h_{12} but we cannot rule out an increase of $\sim 50\text{ cm}^{-1}$ in E_0 .

B. Thermal gas phase

In contrast to the exponential decays observed in solution and to the nearly exponential decays observed in the supersonic expansion, highly nonexponential decay is observed in the isolated thermal samples. In the case of stilbene h_{12} this nonexponential decay was successfully modeled by Balk and Fleming⁵ using the expression

$$I_f(t) = \sum_f D(E_f) \exp[-k(E_f)t], \quad (2)$$

where $k(E_f)$ is the total fluorescence rate out of level f [i.e., $k(E_f) = k_{nr}(E_f) + k_r$, where k_{nr} and k_r are the nonradiative and radiative decays, respectively]. $D(E_f)$ is determined by the Boltzmann distribution in S_0 prior to excitation, by the Franck–Condon factors between levels of S_0 and S_1 and by the spectrum of the excitation pulse. In our previous study of stilbene h_{12} , we made the simplifying assumption that the initial population in S_1 was a Boltzmann distribution shifted by the excess energy above that of the 0–0 transition. In this model the nonexponentiality simply arises from the progressive “cooling” of the ensemble as hot molecules decay by isomerization. The use of Eq. (2) implies complete IVR since energy solely determines the rate and all states contribute. However, if IVR is extensive, the error in using Eq. (2) may be rather small.

The top two curves in Fig. 5 show decays from isolated thermal samples of stilbene h_{12} and d_{12} excited near the origin. The decays are very similar, although the d_{12} curve lies slightly below the h_{12} curve at long times. Figure 11 shows thermal decays calculated via Eq. (2) using the RRKM results of Fig. 9. All the isotopes have very similar initial decays as they must since the initial decay corresponds to the transition state rate,⁵ which is identical for all the molecules given the parameters used in Fig. 9. The d_{10} and d_{12} curves do, however, decay slightly more rapidly than the h_{12} and h_2 curves in the intermediate time regime. In particular, the difference between h_{12} and d_{12} is quite similar to the experimental curves. It might, at first sight, seem odd that the thermal d_{12} system decays slightly faster than the thermal h_{12} system, given that the reverse is true for the microcanonical rates. The reason for this behavior is that the Boltzmann distribution is shifted to higher vibrational energies in d_{12} because of the lower vibrational frequencies. Thus in a thermal sample a larger fraction of the molecules have sufficient energy to cross the barrier to isomerization.

When collisions are introduced by adding methane buffer gas the isomerization rates of h_{12} and d_{12} revert to the order observed in the jet (Fig. 5). Figure 6 shows data for $P \geq 1$ atm for all four molecules. For $P \geq 1$ the h_{12} and d_{10} data are identical within our precision. This trend continues into solution and is consistent with the differing microcanonical

TABLE VII. Arrhenius parameters.

	Hexane	Propanol	MeOH
$h_{12} E_a$ (kcal/mol)	3.82 ± 0.10	4.43 ± 0.06	3.90 ± 0.32
A (s^{-1})	$(7.58 \pm 1.79) \times 10^{12}$	$(3.17 \pm 0.40) \times 10^{13}$	$(1.69 \pm 1.68) \times 10^{13}$
$d_2 E_a$ (kcal/mol)	3.83 ± 0.10	4.66 ± 0.06	3.97 ± 0.32
A (s^{-1})	$(5.25 \pm 1.24) \times 10^{12}$	$(3.61 \pm 0.43) \times 10^{13}$	$(1.33 \pm 1.31) \times 10^{13}$
$d_{10} E_a$ (kcal/mol)	3.80 ± 0.10	4.43 ± 0.08	3.84 ± 0.32
A (s^{-1})	$(7.26 \pm 1.71) \times 10^{12}$	$(3.07 \pm 0.50) \times 10^{13}$	$(1.46 \pm 1.45) \times 10^{13}$
$d_{12} E_a$ (kcal/mol)	3.96 ± 0.45	4.47 ± 0.08	3.98 ± 0.32
A (s^{-1})	$(6.14 \pm 1.57) \times 10^{12}$	$(2.29 \pm 0.35) \times 10^{13}$	$(1.30 \pm 1.27) \times 10^{13}$

rate in the two molecules arising solely from an increased density of states in the d_{10} molecule. Although the nonradiative rate appears to increase linearly with methane pressure, this trend cannot continue because by 5 atm the ratios of rates between h_{12} (or d_{10}) and d_2 or d_{12} have essentially reached their solution values. All the decays appear exponential above 2 atm. The rapid changes in the fluorescence decays over the range 1–5 atm buffer gas pressure can again be explained by a lack of complete IVR in the isolated molecules. In this picture $k_{h_{12}}/k_{d_{12}}$, for example, will reach a constant value when IVR is effectively complete on the isomerization time scale.

Troe and co-workers²⁴ have stressed that changes in the barrier height for isomerization may occur even at very low densities as a result of van der Waals interactions. Their argument stems from the finding that the transition state rate, estimated from either supersonic jet data or RRKM calculations is about ten times smaller than the observed maximum rate.^{16,17} While we do not wish to rule out the importance of solvent shifts, it is not clear why there would be differing effects between d_{12} and h_{12} , for example, as methane pressure increases from 0 to 5 atm, whereas from 5 to 100 atm the curves change in a parallel fashion (Fig. 6). In addition, if

IVR is incomplete in the isolated molecule, estimates of k_{TSR} from the experimental data or from RRKM calculations that have been parametrized to fit the jet data are not secure.

IV. CONCLUDING REMARKS

The ordering of the microcanonical decay rates of the *t*-stilbene isotopes h_{12} , d_2 , d_{10} , d_{12} does not conform to the predictions of RRKM theory, in either of the forms that have been used previously to describe the h_{12} data.^{1,3}

A model based on extensive but not complete IVR in the isolated molecule, which rapidly becomes complete as buffer gas is added, seems qualitatively compatible with all our data. Further studies of IVR are clearly required in order to test this model.

ACKNOWLEDGMENTS

This work was supported by Grant Nos. NSF CHE 83-03997 and NSF CHE 83-11971. We thank Silvio Canonica for assistance with the gas phase measurements, S. Nordholm and J. Jean for assistance with the RRKM calculations, and Professor N. C. Yang for helpful discussions.

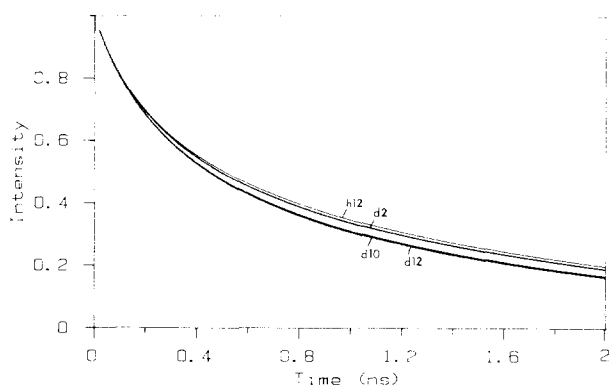


FIG. 11. Thermal isolated molecule decays for the stilbene isotopes calculated from the data of Fig. 9.

- ¹J. Troe, Chem. Phys. Lett. **114**, 241 (1985).
- ²J. Schroeder and J. Troe, J. Phys. Chem. **90**, 4215 (1986).
- ³P. M. Felker and A. H. Zewail, J. Phys. Chem. **89**, 5402 (1985).
- ⁴J. A. Syage, P. M. Felker, and A. H. Zewail, J. Chem. Phys. **81**, 4685, 4706 (1984).
- ⁵M. W. Balk and G. R. Fleming, J. Phys. Chem. **90**, 3975 (1986).
- ⁶S. H. Courtney and G. R. Fleming, J. Chem. Phys. **83**, 215 (1985).
- ⁷G. R. Fleming, S. H. Courtney, and M. W. Balk, J. Stat. Phys. **42**, 83 (1986).
- ⁸G. Maneke, J. Schroeder, J. Troe, and F. Voss, Ber. Bunsenges. Phys. Chem. **89**, 896 (1985).
- ⁹K. N. Campbell and L. T. Eby, J. Am. Chem. Soc. **63**, 216 (1941).
- ¹⁰A. T. Blomquist, L. H. Liu, and J. C. Bohrer, J. Am. Chem. Soc. **74**, 3643 (1952).
- ¹¹R. E. A. Dear and F. L. M. Patterson, J. Am. Chem. Soc. **85**, 662 (1963).
- ¹²M. C. Chang, S. H. Courtney, A. J. Cross, R. J. Gulotty, J. W. Petrich, and G. R. Fleming, Anal. Instrum. **14** (3 and 4), 433 (1985).
- ¹³L. A. Philips and D. H. Levy, J. Chem. Phys. **85**, 1327 (1986).
- ¹⁴L. A. Philips, S. P. Webb, S. J. Martinez III, G. R. Fleming, and D. H. Levy, J. Am. Chem. Soc. **110**, 1352 (1988).
- ¹⁵T. J. Majors, U. Even, and J. Jortner, J. Chem. Phys. **81**, 2330 (1984).
- ¹⁶M. Lee, G. R. Holtom, and R. M. Hochstrasser, Chem. Phys. Lett. **118**,

- 359 (1985).
- ¹⁷V. Sundstrom and T. Gillbro, *Chem. Phys. Lett.* **109**, 538 (1984).
- ¹⁸S. H. Courtney, Ph.D. thesis, The University of Chicago, 1987.
- ¹⁹S. K. Kim and G. R. Fleming, *J. Phys. Chem.* **92**, 2168 (1988).
- ²⁰J. Troe and K. M. Weitzel, *J. Chem. Phys.* **88**, 7031 (1988).
- ²¹Z. Meic and H. Gusten, *Spectrochim. Acta Part A* **34**, 101 (1978).
- ²²A. Warshel, *J. Chem. Phys.* **62**, 214 (1975).
- ²³L. H. Spangler, R. D. van Zee, S. C. Blankespoor, and T. S. Zwier, *J. Phys. Chem.* **91**, 6077 (1987).
- ²⁴J. Schroeder and J. Troe, *Ann. Rev. Phys. Chem.* **38**, 163 (1987).